



Inclusion of Broadband Shock-Associated Noise in Spectral Decomposition of Noise from High-performance Military Aircraft

Tracianne B. Neilsen,¹ Aaron B. Vaughn,² Kent L. Gee,³ S. Hales Swift⁴
Brigham Young University, Provo, UT, 84602

Alan T. Wall⁵
Air Force Research Laboratory, Wright-Patterson Air Force Base, OH, 45433

and

J. Micah Downing⁶ and Michael M. James⁷
Blue Ridge Research and Consulting, LLC, Asheville, NC 28801

Attempts to reduce the noise from high-performance military aircraft requires an understanding of the different jet noise generation mechanisms. The primary noise sources originate from interactions between turbulent mixing noise associated with large and fine-scale turbulent structures and the ambient air. A nonideally expanded jet also contains broadband shock-associated noise. A three-way decomposition of the spectral density measured near a tied-down F-35B quantifies the contribution from each type of noise. The decomposition is performed on noise from a ground-based, linear array of microphones, approximately 8 m from the estimated shear layer, which spanned an angular aperture of 35° to 152° (relative to engine inlet). This large spatial aperture allows for a detailed investigation into the spatial variation in broadband shock-associated noise and fine and large-scale turbulent mixing noise. The spectral decompositions match the measured spectral levels with three main exceptions: 1) the F-35B noise contains multiple spectral peaks in the maximum radiation region, 2) nonlinear propagation increases the high-frequency spectral levels, and 3) the low-frequency levels in the maximum radiation region are less than those predicted by the large-scale similarity spectrum. The main peak of the F-35B broadband shock-associated noise, evident from 35°-70°, has the same characteristic shape and variation in peak frequency as overexpanded, laboratory-scale jets. The F-35B broadband shock-associated noise peak level and width exhibit different trends than laboratory-scale BBSAN and those recently reported for the F/A-18E [Tam *et al.*, *Journal of Sound and Vibration*, Vol. 422, 2018, pp. 92-111]. The strengths and limitations of current models to represent the spatial variation in the spectral content of F-35B noise can guide research efforts to more fully understand the sound radiation from high-performance military aircraft.

¹ Associate Professor, Dept. of Physics and Astronomy, N283 ESC, AIAA Member.

² Undergraduate Student, Dept. of Physics and Astronomy, N283 ESC.

³ Professor, Dept. of Physics and Astronomy, N283 ESC, AIAA Senior Member.

⁴ Postdoctoral Fellow, Dept. of Physics and Astronomy, N283 ESC, AIAA Member.

⁵ Research Physicist, Battlespace Acoustics Branch, Air Force Research Laboratory, 2610 Seventh St., Bldg. 441, Wright-Patterson AFB, OH 45433, AIAA Member, AIAA Member.

⁶ President and Chief Scientist, 29 N Market St, Suite 700, AIAA Member.

⁷ Sr. Vice President and Chief Engineer, 29 N Market St, Suite 700, AIAA Member.

Nomenclature

c	=	ambient sound speed
D	=	nozzle diameter
E_j	=	amplitude based on jet parameters
f	=	frequency
f_m	=	modal frequency
f_{peak}	=	peak frequency
J	=	Bessel's function of the first kind
k	=	acoustic wavenumber
k_m	=	modal wavenumber
L	=	shock-cell spacing
L_{peak}	=	peak spectral level
M_c	=	convective Mach number
M_d	=	design Mach number of the nozzle
M_j	=	average Mach number of the fully expanded jet
m	=	mode number
OASPL	=	overall sound pressure level
PSD	=	power spectral density
R	=	radius in spherical coordinates
S	=	spectrum
SPL	=	sound pressure level
Sr	=	Strouhal number
u_c	=	convective velocity
u_j	=	fully expanded, mean jet velocity
w_{sh}	=	width parameter
x	=	sideline distance
z	=	axial distance
ΔSPL	=	difference in sound pressure level
β	=	jet offdesign parameter
ϕ	=	azimuthal angle
θ	=	polar inlet angle
σ	=	zero of zeroth order Bessel function

I. Introduction

NOISE reduction efforts for the latest generation of tactical aircraft are of increasing importance to both the military and the civilian population. Noise reduction designs can benefit from an increased understanding of each noise component and their relative importance at different operating conditions. The noise generation mechanisms fall into two categories: turbulent mixing noise and broadband shock-associated noise. In the two-source theory for turbulent mixing noise [1,2,3], the maximum noise generation is caused by the large-scale turbulent structures' interaction with the ambient air; the partially correlated nature of these interactions yields the distinct directivity associated with supersonic jet noise. Fine-scale turbulent structures also interact with the ambient air to produce lower-level, omnidirectional noise. Because high-performance military aircraft engines do not produce an ideally expanded jet, broadband shock-associated noise (BBSAN) is also a significant component of the noise in the sideline and forward direction. BBSAN results from the interaction of the large-scale turbulent structures and the quasi-periodic shock cells [4]. Screech tones, while important in laboratory-scale underexpanded jets [5] are not significant in overexpanded jets nor the spectra from high-performance military aircraft. The relative importance of the BBSAN and the large and fine-scale turbulent mixing noise is explored across a wide spatial aperture near the F-35B via a three-way spectral decomposition. This decomposition includes variation with engine power and provides insights into where current models, developed for laboratory-scale jet noise, apply to high-performance military

aircraft noise. This spectral decomposition helps identify where further investigation into noise source mechanisms are needed and lays the ground work for the development of a broadband equivalent source model for F-35B noise.

In the two-source theory of jet noise, different kinds of turbulent mixing noise come from fine and large-scale turbulent structures [1,2]. An experimental study of supersonic jet noise reported by Schlinker [6] and Laufer *et al.* [7] in the mid 1970's indicated that the sound radiated to the sideline of a jet and in the highest amplitude region are distinctly different. The two regions contain noise generated by the fine and large-scale turbulent structures and have different properties. The fine-scale turbulent structures distributed throughout the plume, are relatively compact sources and radiate omnidirectionally. The large-scale turbulent structures have larger spatial coherence properties and thus produce directional sound radiation. Consequently, in the direction of maximum radiation, noise from the large-scale structures dominates the sound field. The noise radiated from the fine-scale structures is, therefore, most likely to be detected to the sideline of the jet. The relative contribution of these two noise sources depends on Mach number, jet temperature, and radiation angle [8,9].

Studies of these two types of mixing noise led to the empirical similarity spectra, developed from far-field data from a range of cold and heated, ideally expanded, laboratory-scale jets [10,11]. The large-scale similarity (LSS) spectrum, which has a relatively narrow peak and power-law decay on both sides, was reported to fit the jet noise for aft angles, where the sound radiation is a maximum. On the other hand, the fine-scale similarity (FSS) spectrum—with its broader peak and a more gradual roll-off at both high and low frequencies—matched the spectra of noise radiated in the sideline and forward directions. In addition, it was proposed that the turbulent mixing noise at any radiation angle is a sum of LSS and FSS spectra. The agreement between the similarity spectra and laboratory-scale jets at a variety of operating conditions is summarized in Refs. [8,9,12]. Schlinker [13] first applied the LSS spectrum to noise in the maximum radiation direction from a high-performance military aircraft engine. Neilsen *et al.* [14] contains the first comparison of both the FSS and LSS spectra to noise measured on ground-based microphones spanning a wide angular aperture close to a tied-down high-performance military aircraft. It was shown that the similarity spectra agree with the measured turbulent mixing noise with a few important exceptions, explained in Sec. II.A. Spectral comparisons have also been shown for a few elevated microphones 38.1 m from a tied-down F-35AA1 [15] and recently for a few ground-based microphones near a tied-down F/A18-A/E [16]. In addition, Harker *et al.* [17,18] explain how the autocorrelation envelopes associated with the similarity spectra agree with the measured autocorrelation near the high-power, installed engine in Ref. [14]. Recently, Faranosov *et al.* [19] compared the similarity spectra to an azimuthal decomposition of an aircraft engine on a static test bench. All of these studies have focused solely on the turbulent mixing noise.

In addition to turbulent mixing noise, nonideally expanded jets produce BBSAN. Harper-Bourne and Fisher [4] first identified the primary features of BBSAN (distinctive spectral shape, peak frequency, and peak level) and provided a methodology for predicting these features based on constructive interference due to the relative phasing of the sources. A series of laboratory-scale experiments at the NASA Langley Research Center [20,21,22], confirmed the presence of and spatial variation in these three BBSAN features. Tanna [23] explored the relative importance of BBSAN to turbulent mixing noise. BBSAN becomes stronger as the jet Mach number, M_j , deviates more from the design Mach number, M_d . BBSAN is evident in the forward quadrant (small inlet angles) where the turbulent mixing noise has lower levels. The prominence of BBSAN relative to turbulent mixing noise decreases when temperature increases because of the corresponding increase in turbulent mixing noise. After additional experimental results that explored the shock-turbulence interactions [21], evaluated the BBSAN spectral shape [24], and investigated the role of shock structures and jet mixing layer development [25], Tam and colleagues [26,27,28] proposed a more sophisticated BBSAN spectral model. More recently Kuo *et al.* [29] provided a simplification of Tam's model that works well for the first spectral peak.

The nature of BBSAN in high-performance military aircraft noise is now under investigation. Tam *et al.* [16] modeled the BBSAN at a few locations near a tied-down F/A-18E operating at afterburner and reported that BBSAN from a high-performance military aircraft agrees with only two of the four trends observed in nonideally expanded, laboratory-scale jets. They indicated that the distinctive BBSAN spectral shape is present and that the spectral peak frequency increases as inlet angle increases for seven locations. Four of these seven locations show opposite trends from laboratory-scale studies in the BBSAN peak level and width. Vaughn *et al.* [30] show the first analysis of BBSAN characteristics as a function of engine condition for a high-performance aircraft engine. Specifically, the BBSAN characteristics are compared when the F-35B operated at four engine conditions: 75% engine thrust request (ETR), 100 % ETR (military power), 130% ETR (minimum afterburner), and 150% ETR (maximum afterburner). The F-35B BBSAN spectral shape and trend in peak frequency hold for all four engine conditions. The expected

variations in peak frequency across engine condition also agree with prior laboratory-scale studies in which the temperature and Mach number were varied [29]. The variation in peak level and width do not agree with laboratory-scale studies nor the F/A-18E study. A direct comparison between the F/A-18E and F-35B BBSAN characteristics for afterburning engine condition are presented in this paper.

With the goal of increasing understanding of the noise generation mechanisms from an F-35B engine operated at different engine conditions, this paper presents a comprehensive, three-way spectral decomposition of F-35B noise over a wide angular aperture and multiple engine conditions. In addition to confirming the strengths and limitations of applying the large and fine-scale similarity spectra to the F-35B noise, particular attention is given to examining if the dominant BBSAN peak in the F-35B spectra can be modeled using the prevailing theory. After an explanation of the spectral models (Sec. II), a brief description of the measurements is given (Sec. III). Examples of the three-way decomposition are provided (Sec. IV) from the 71-element ground array, which spanned 32 m and was located approximately 8-10 m from the estimated shear layer. The spectral decompositions are analyzed (Sec. V) at both 75% engine thrust request (ETR) and 150% ETR (maximum afterburner). Spatial variation in level and peak frequency for all three components shows the relative contributions of each. Broadband spatio-spectral error maps highlight regions in which the three spectral models do and do not adequately match the F-35B spectra. In addition, the spatial variation in the BBSAN modeling parameters are compared to those reported for the F/A-18E. The applicability of the standard relationship between the BBSAN peak frequency and the convective speed is evaluated, followed by a preliminary look at using the Kuo *et al.* model to account for a second BBSAN peak. These analyses provide insights into the relative significance of the different jet noise components for an F-35B operating at different ETR and how these agree and disagree with prior conclusions.

II. Background

The majority of the spectral decomposition has been used for jet noise component identification. Prior studies have applied either the Tam *et al.* similarity spectra for turbulent mixing noise or modeled the BBSAN components separately. In Ref. [31], however, Viswanathan *et al.* proposed a different spectral method for separating turbulent mixing noise and BBSAN, based on the work in Ref. [32]. Spectral scaling laws were applied to a large database of jet noise measurements, and found a consistent spectral shape could be obtained over a range of known jet velocities and temperatures. Master spectra were created for turbulent mixing noise from ideally expanded, subsonic jets using a least-square fit of the scaled spectra at different temperature ratios. The master spectra were scaled to fit ideally expanded, supersonic jet noise spectra at the same temperature using the jet velocity and velocity scaling exponent. He noted that master spectra did not match the high-frequency content of supersonic jet noise spectra because of nonlinearity. In Ref. [31] (Figs. 8, 9, 12, and 13), these master spectra were subtracted from supersonic jet noise containing BBSAN to yield the “shock component.”

The Viswanathan *et al.* scaling-law approach [31] is not used to decompose the F-35B noise for several reasons. First, the jet temperature and velocity are not known for the F-35B. Second, the master spectra shown in Ref. [31] have a peak Strouhal number around 0.2, which is expected in the maximum radiation region but not at the forward angles where BBSAN is prominent. An example of the spatial variation in the peak frequency for a high-performance military aircraft engine is provided in Ref. [33]. Third, the “shock component” contains not only the BBSAN but also energy related to nonlinear propagation, as discussed by Viswanathan *et al.* in regards to Figs. 34-35 of Ref. [31]. Supporting evidence for this claim was presented by Petitjean *et al.* [5] in their detailed study of nonlinear propagation effects at small inlet angles for supersonic, imperfectly-expanded, heat-simulated model jets.

Because of these considerations, the Tam *et al.* empirical similarity spectra for turbulent mixing noise [10] and Kuo *et al.*'s BBSAN model [29] are used to identify the contributions of the different noise sources. These two spectral models are described in this section.

A. Similarity Spectra for turbulent mixing noise

Two empirical similarity spectra obtained by Tam *et al.* [10] match the primary features of the mixing noise from the fine-scale and large-scale turbulent structures in many laboratory-scale jet noise studies [8,9]. These spectra depend on two input parameters: peak frequency and peak level. An example of the two spectra when the same peak frequency and level are used is shown in Figure 1, based on the corrected equations found in Ref. [11], with the LSS spectrum corresponding to the F function and the FSS spectrum the G function.

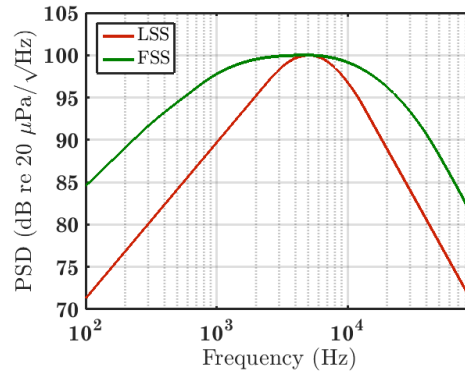


Figure 1. Large-scale and fine-scale similarity spectra for the same peak frequency and peak level.

Comparisons of the similarity spectra and spectra from high-performance military aircraft engines are limited. In the investigation by Schlinker *et al.* [13], the LSS spectral shape agrees reasonably well with the measured spectra at aft angles in the far field of a round-nozzle engine at its full-thrust set point, except for high frequencies where the spectral slope was appreciably shallower than predicted by the LSS spectrum. Neilsen *et al.* [14] were the first to compare both the FSS and LSS spectra, and their combination, against the spectra from a tied-down high-performance military aircraft. [34] They evaluated the ability of one-third octave band similarity spectra to match spectral levels on ground-based microphones located 11.7 m (approximately 18 nozzle diameters, D) from the jet centerline that spanned a wide angular aperture. Even though the engine nozzle geometry was non-circular for this aircraft and one engine ran at idle power while the other engine cycled through different engine conditions, the similarity spectra agree with large portions of the measured spectra. Toward the sideline of the aircraft, the fine-scale similarity spectrum agrees well, while the large-scale similarity spectrum provides a reasonable fit to the general shape around the area of maximum radiation, with a few important exceptions. Combinations of the two similarity spectra are shown to match the data in between those regions. Surprisingly, at high engine powers, a combination of the two similarity spectra is also evident at the farthest aft microphones with inlet angle around 150° .

There are three main features in high-performance military aircraft spectra that are not accounted for by the similarity spectra. First, at high frequencies, the degree of congruity between the similarity and measured spectra changes with engine condition and angle. At high engine powers, the measured high-frequency slope is systematically shallower than the LSS spectrum [35], with the largest discrepancy occurring in the region of maximum radiation. The shallowness of the high-frequency slope—apparent even in the forward direction—is due to nonlinear propagation. [33,36,37,38,39]. This effect was often ignored in previous laboratory-scale studies in which the fit in the peak frequencies was sacrificed to compensate for the steeper slope, whereas in this work frequencies below 2000 Hz were primarily considered in fitting the similarity spectra in the maximum radiation region.

Second, the LSS spectrum does not account for the presence of multiple spectral peak found in high-amplitude regions. Seiner *et al.* [40] showed a dual lobe for very high-temperature laboratory-scale jets and attributed it to different types of Mach waves described by Oertel [41] with theoretical modeling provided by Tam and Hu [42]. For the one-third octave band analysis of military aircraft engine noise in Ref. [14], only two spectral peaks are evident, but subsequent studies have indicated there are likely more [43,44,45]. More recently, Liu *et al.* [46] has shown a similar separation of different types of propagating waves in numerical simulations of high temperature, supersonic jets.

Third, the measured low-frequency spectral slope is steeper than is predicated by the LSS spectrum at in the maximum radiation region. Farther aft the two-frequency slope changes and agrees better with the similarity spectral decomposition. The steeper low-frequency slope persists in the far field, as shown in Figs 4 and 5 of Gee *et al.* [37] No explanation for this phenomenon has been proposed.

These conclusions were further investigated in a preliminary comparison of one-third octave band similarity spectra to the spatial variation in spectra which was performed for elevated microphones on an arc at a radial distance of 38.1 m from the F-35AA1 [15]. While the resulting one-third octave band spectral decomposition appeared to agree with the previous aircraft noise decomposition [14], the decomposition in Ref. [15] was complicated by the presence of a ground interference dip near the peak frequency. Thus, confirmation of the similarity spectra's ability to match high-performance military aircraft noise is more straightforward for a ground-based array, as was present in

2013 measurements near tied-down F-35B [47]. Examples of spectral decompositions along this ground array are shown in Sec. IV.

B. BBSAN models

In Ref. [4], Harper-Bourne and Fisher first proposed a methodology for predicting BBSAN. Each shock cell is treated as a source with relative phasing set by the convective velocity of the turbulent flow. This led to an expression for a BBSAN spectral shape and, in particular, the relationship between the peak frequency of the BBSAN, the convective Mach number, and the length of the shock cells. They concluded that the level of BBSAN depends only on pressure ratio. The BBSAN intensity was observed to go as β^4 , with $\beta = \sqrt{M_j^2 - 1}$ (for their convergent nozzle).

For convergent-divergent nozzles, Ref. [26] indicates that the appropriate definition is $\beta = \sqrt{M_j^2 - M_d^2}$. The relationship between β^4 and the level of the BBSAN indicates a strong dependence on the density fluctuations at the shocks.

Harper-Bourne and Fisher [4] also postulated that the peak frequency, f_p , associated with the maximum BBSAN level is related to convective velocity, u_c , convective Mach number, M_c , and average shock-cell spacing, L . At a specific observation angle θ , relative to the jet centerline, the radiation from all the shock-cell sources would interfere constructively at the frequency

$$f_p = \frac{u_c}{L(1 - M_c \cos\theta)} \quad (1)$$

and harmonics of f_p . The upper harmonics, however, were not observed in their measurements. They also proposed a spectral model based on flow parameters. The Harper-Bourne and Fisher model for BBSAN was tested with several lab-scale experiments. Tanna's experiments confirmed that the BBSAN increases as β increases [23]. Norum and Seiner's experiments compared BBSAN measurements over a showed that the Helmholtz number associated with f_p increases with β for overexpanded jets [21]. The distinctive shape of the BBSAN peak rise as f^4 below f_p and decay as f^{-2} above f_p , as shown by Pao and Seiner [24].

A later BBSAN model was developed from instability wave theory for the large-scale turbulent mixing noise by Tam and colleagues [26,27,28]. In the Tam model, BBSAN is produced by the coherent scattering of the large turbulence structures as they pass through the quasi-periodic shock cells in the jet plume. Interaction between the large-scale turbulence structures and the quasi-periodic shock cells gives rise to time-dependent disturbances, which when radiated to the far field become BBSAN. In essence, the quasi-periodic shock cells form a waveguide for the large-scale turbulent structures. It was noted that quasi-periodic shock cells first increase then decrease as β increases. Additionally, the intensity of BBSAN depends on the strength of the shock cells inside the plume, and shock cell strength is determined by the difference between the nozzle design Mach number, M_d , and the fully expanded jet Mach number, M_j . In Ref. [28], the model was extended from the original derivation for slightly imperfectly expanded jets to moderately imperfectly expanded jets.

In the Tam model for moderately imperfectly expanded jets, the far-field BBSAN spectrum (Eq. 3.7 in Ref. [28]) depends on frequency, f , and location in spherical coordinates (R, θ, ϕ) . A more compact version is presented here, where E_j represents a collection of ambient and jet parameters:

$$S(R, \theta, \phi, f) = \frac{E_j}{R^2 f S r_f} \left[\sum_{m=1}^{\infty} \frac{1}{\sigma_m^2 J_1^2(\sigma_m)} \exp \left\{ - \left(\frac{f_m}{f} - 1 \right)^2 \right\} q(\theta)^2 \right], \quad (2)$$

with

$$q(\theta)^2 = (1 + M_c \cos\theta)^2 \frac{L^2 u_j^2}{u_c^2 (2 \ln 2)}. \quad (3)$$

The use of E_j is employed here because the jet parameters are not available for high-performance military aircraft engines. This abbreviated form is also convenient because it ties more directly with the subsequent simplifications by Kuo *et al.* [29]. The Sr_f in the denominator is the Strouhal number ($Sr = fu_j/D$) if $St > 0.35$, otherwise $Sr_f = 0.35$, and θ is measured relative to the jet centerline, and J_1 is the first order Bessel function of the first kind.

The summation over m represents the contribution of different waveguide modes to BBSAN. Each term in the sum depends on σ_m , the m^{th} zero of J_0 , as well as $J_1(\sigma_m)$. The exponential term depends on the peak frequency of the m^{th} waveguide mode, f_m , and has angular dependence that varies with M_c . L is the ‘‘half-width of the similarity sources’’ [26,27], and u_j and u_c are the jet and convective velocities. Refs. [26,27] state that in practice the summation is truncated to include only f_m corresponding to $St \leq 3$ because the wave model of large-scale turbulent structures is not meaningful for $St > 3$. He also notes that the modal frequencies occur at $f_m = u_c k_m / (2\pi(1 - M_c \cos \theta))$, where the wavenumbers of the vortex shock cell structure are $k_m = 2\sigma_m / (D_j \sqrt{M_j - 1})$. This equation for peak frequency resembles the one used by Harper-Bourne and Fisher in Eq. (1), but the upper partials are not harmonically related.

While the Tam model allows for the prediction of multiple BBSAN peaks, it has some limitations. When the model is applied to match measured BBSAN spectra, the required f_1 is usually greater than the first observed BBSAN peak frequency, making it tricky to apply the model. In addition, the modeled BBSAN spectrum exhibits more high-frequency partials than observed in measurements, as well as deeper dips between subsequent harmonics [26].

In many cases, only the first peak of BBSAN is identifiable. This observation led Kuo *et al.* [29] to produce a simplified model for the primary BBSAN spectral peak. At (R, θ, ϕ) the contribution of the main BBSAN peak to the sound pressure level is

$$L_{\text{BBSAN}} = L_{\text{peak}} + 10 \log \left(\exp \left[- \left(\frac{f_{\text{peak}}}{f} - 1 \right)^2 / w_{\text{sh}}^2 \right] \right), \quad (4)$$

where the original Strouhal numbers have been replaced by frequencies, as the jet diameter and velocity are unknown for the F-35. L_{peak} is the peak spectral level (SPL or PSD) in decibels that occurs at the peak frequency, f_{peak} . The parameter w_{sh} relates to the width of the BBSAN peak and is typically chosen to match the spectral level at $f = 0.75f_{\text{peak}}$. The advantages of this simplified model are that jet-related parameters are not necessary and identification of L_{peak} and f_{peak} are straightforward. (As a point of clarification, Eq. (4) was referred in a recent publication [16] as Tam’s model, but will be referred to here as Kuo *et al.*’s model.)

A comparison of the spectral shape of Tam’s original model from Ref. [28] and Kuo *et al.*’s model from Ref. [29] illustrates the benefits of the simplification. The spectral shape from both BBSAN models is shown in Figure 2a for the same width and peak frequency: $1/q = w_{\text{sh}} = 0.2$, $f_1 = f_{\text{peak}} = 500$ Hz, with $m = 1$, $E_j = 6.3e7$, $R = 10$ m in Eq. (2) and $L_{\text{peak}} = 100$ dB in Eq. (4). The spectral shapes differ but alternate choices for the peak frequency and the width make them appear similar, as shown Figure 2b where $1/q = 0.2$, $f_1 = 525$ Hz, for the Tam model and $w_{\text{sh}} = 0.185$, $f_{\text{peak}} = 500$ Hz for the Kuo model. In application of BBSAN spectral models, only the top 15-20 dB are usually employed as the elongated tails are not representative of measured spectra [29]. Thus, Kuo *et al.*’s model is selected in this work because it is easier to use: The peak frequency and peak level are easily identifiable, whereas the f_1 required to get reasonable fits in Tam’s model is lower than the actual measured peak frequency and the jet parameters required for Tam’s model are not available for the F-35B.

Both the Harper-Bourne and Fisher model [4], and the original Tam model [26,27], predict the presence of higher-frequency BBSAN components. Although the higher components are not seen in much of the laboratory-scale data, the F-35B data do exhibit a second peak at some inlet angles. Harper-Bourne and Fisher [4] describe the higher partials as harmonics based on constructive interference. Tam’s model includes inharmonic higher frequency partials as modes of the waveguide created by the shock cells [26,27]. The authors of this paper find the latter does not agree with the second peak in the F-35B data. Instead, we are investigating possible relationships between the first and high-order peaks; preliminary evidence is presented in Sec. V.E.

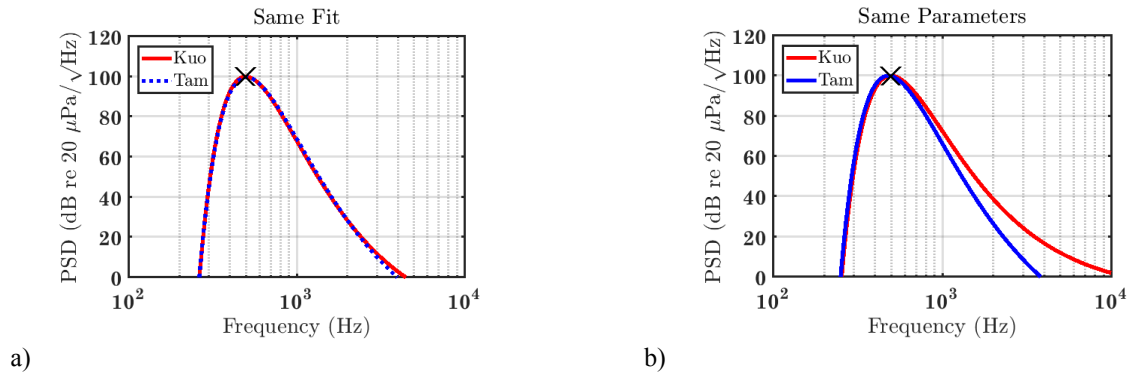


Figure 2. Comparison of the spectral shape of Tam's original model for $m = 1$ in Ref. [28] and Kuo *et al.*'s simplified model in Ref. [29] using the same parameter (a) and different parameters (b). Parameter values are given in the text.

III. Measurement

Noise from a tied-down F-35B was measured at Edwards Air Force Base, September 6, 2013. The Pratt & Whitney F135 engine was operated at a series of engine conditions from idle to 150% engine thrust request (ETR). Each engine condition was measured multiple times and produced consistent spectra. Microphones were arranged in either line arrays, parallel to the jet centerline, or in semicircular arcs centered at the microphone array reference point (MARP), described by James *et al.* [47]. As most of the noise generated by supersonic jets is emitted from the turbulent mixing that occurs behind the jet, the MARP represents a rough estimate of source location for many frequencies of interest, and is used to define angles. Measurements were conducted in the early morning hours, with temperature varying between 19.4°C and 23.1°C, relative humidity between 37.6% to 45.7%, and an average wind speed of 3.3 kts. Two variants of the F-35 were measured, and as reported in Ref. [47] the sound from the F-35A and F-35B share the same characteristics. Nonlinear propagation effects across near to far-field arrays were analyzed in Refs. [48] and [49]. In addition to the far and mid-field arrays, a ground-based array was deployed closer to the aircraft.

The results and analyses in this paper come from noise measured on the 71-element, ground-based, linear array of microphones. This linear array was approximately 8-10 m from the estimated shear layer of an F-35B. The array spanned 32 m, corresponding to an angular aperture of 35°-152° relative the engine inlet and the MARP, as illustrated in Figure 3. The 6.35 mm (1/4") diameter microphones were spaced 0.45 m (18") apart. Calibrated acoustic pressure waveform data were synchronously acquired with National Instruments PXI-4498 cards sampling at 204.8 kHz. Five or six measurements were taken at each ETR, and the variation in the measured levels was less than 1 dB. The ground-based linear array provides the opportunity to analyze the spatial variation in F-35B power spectral density (PSD) without interference from ground reflections. These data are used in several concurrent studies, including a correlation and coherence analysis [45] and acoustical holography [44].

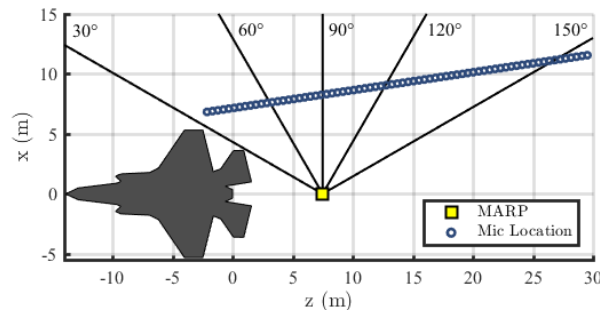


Figure 3. Measurement schematic of the ground-based, 71-element linear array, approximately 8 m from the estimated shear layer. Inlet angles are measured relative to the MARP (microphone array reference point).

IV. Results

The similarity spectra decompositions for F-35B jet noise from the ground-based linear array lend insights into the applicability of the current spectral models. As noted by Morris [50], there is some leeway in defining the parameters that match the similarity spectra to measured spectral shapes. In this case, three guidelines are applied. First, the decompositions primarily strive for agreement in the peak-frequency region. Second, the contributions to the OASPL associated with the BBSAN, FSS, and LSS spectral components are constrained to grow or decay smoothly as a function of inlet angle. Third, the peak frequency of each spectrum is expected to vary smoothly as the inlet angle increases. Examples of similarity spectra fits are shown in Figure 4 through Figure 6 for select microphones when the engine was operated at 75% ETR.

The spectral decompositions at 75% ETR capture much of the spatial variation in the F-35B noise, with the same notable exceptions observed for a different high-performance military aircraft [14]. At the smallest inlet angles, the PSD contains BBSAN. A combination of Kuo *et al.*'s BBSAN model in Eq. (4) and the FSS spectrum matches the majority of the spectral shape, as shown in Figure 4(a). As the inlet angle increases, the relative strength of the BBSAN decreases while the turbulent mixing noise associated with the fine-scale turbulent structures increases. As the inlet angle passes approximately 76° , the BBSAN is no longer evident, and the FSS spectrum matches the PSD, as displayed in Figure 4(b). The "FSS only" condition spans a very narrow angular range for 75% ETR; at approximately 80° the LSS spectrum must be added in to reproduce the spectral shape (Figure 5(a)). This combination region extends to approximately 105° , after which the addition of FSS spectrum no longer improves the agreement, and the LSS spectrum matches all except the high frequencies (Figure 5(b)), which have elevated levels due to nonlinear propagation [48,49]. In the maximum radiation region (inlet angles approximately 110° - 140° at 75% ETR), the LSS spectrum captures the overall shape of the peak region of the PSD (Figure 6(a)), but misses several important features: 1) multiple spectral peaks [43,44,45], 2) shallower high-frequency slope (of $1/f^2$) resulting from nonlinear propagation [36,37,38,39,48,49], and 3) steeper low-frequency slope. All three features were noted in prior spectral decompositions of high-performance military aircraft [14,15,33], and are discussed in more detail in Sec. V.B. Beyond the maximum radiation lobe, the PSD high-frequency slope steepens and better matches the LSS spectrum (Figure 6(b)). Then, at larger angles, for high ETR, the high-frequency spectral shape shifts again, and a better match to the PSD can be achieved when a combination of the LSS and FSS spectra is used. This was first shown for a different high-performance aircraft engine one-third octave band spectra in Figure 8 of Ref. [14] and then at a closer location in Figure 8 of Ref. [33]. It is hypothesized that the fine-scale turbulent structures radiate omnidirectionally and are apparent in the spectral shape aft of the maximum radiation lobe, when both the level and, perhaps more importantly, the peak frequency of the large-scale turbulent structures are lower. Analysis of spatial trends of the three-way spectral decomposition give insights into how the models for turbulent mixing noise and BBSAN spectra do and do not agree with spectral levels from the F-35B at different ETRs.

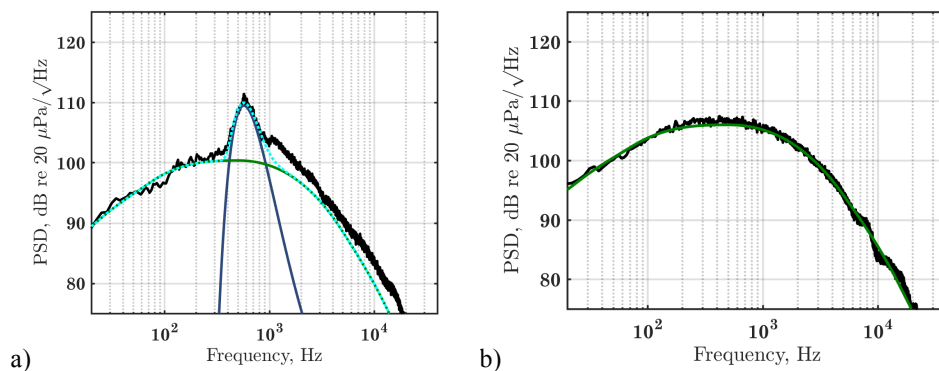


Figure 4. F-35B PSD at 75% ETR (black) at inlet angles of (a) 35° and (b) 76° compared to the FSS spectrum (green), Kuo *et al.*'s BBSAN model (blue) and the total modeled PSD (cyan).

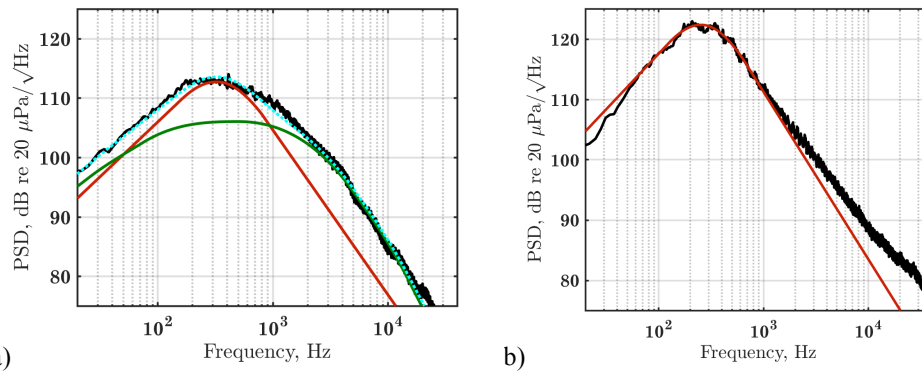


Figure 5. F-35B PSD at 75% ETR (black) at inlet angles of (a) 92° and (b) 117° compared to the FSS (green) and LSS (red) spectra and the total modeled PSD (cyan)

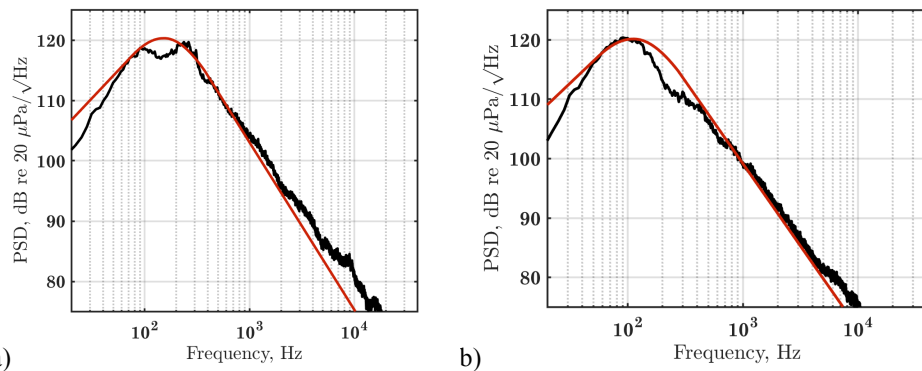


Figure 6. F-35B PSD at 75% ETR (black) at inlet angles of (a) 133° and (b) 146° compared to the LSS (red) spectrum.

V. Analyses

A. Characteristics of the spectral decomposition

The three-way spectral decomposition was performed at all 71 locations of the ground-based linear array near a tied-down F-35B. While there is latitude in fitting the spectral models to the PSD, the fits were guided by the goal of creating the best fit in the peak-frequency portion of each spectrum while maintaining smoothly varying OASPL and peak frequency, as described in Sec. IV. The contributions of each spectral component to the OASPL is displayed in Figure 7, along with the measured OASPL as a function of inlet angle. An outward spherical spreading correction is applied to scale the OASPL to a common distance of 30 m from the MARP; the spherical spreading assumption is reasonable in this case because the OASPL is dominated by frequencies not affected by the nonlinear propagation. At 75% ETR, the contribution to the OASPL from the FSS and LSS spectra increases and decreases as inlet angle increases with the maximum contribution of the FSS spectrum occurring at inlet angles of 75°-100° (relative to the MARP). At 150% ETR, similar trends are seen in the FSS and LSS levels. In both cases, the OASPL of the LSS component agrees with the measured OASPL in the relatively large maximum radiation region but does so by splitting the difference between the multiple spectral peaks, as illustrated in Figure 6(a). The relative contribution of BBSSAN to the combined OASPL decreases as inlet angle increases and the turbulent mixing noise becomes more prominent. However, a difference is observed between 75% ETR and 150% ETR. The decrease in level with inlet angle, as at 75% ETR, agrees with prior laboratory-scale studies, while the slight increase seen at 150% ETR does not. This difference has been examined in Ref. 30 and is considered in Sec. IV.C. The spatial variations in the three spectral models' contributions to the OASPL follows smoothly varying, expected trends.

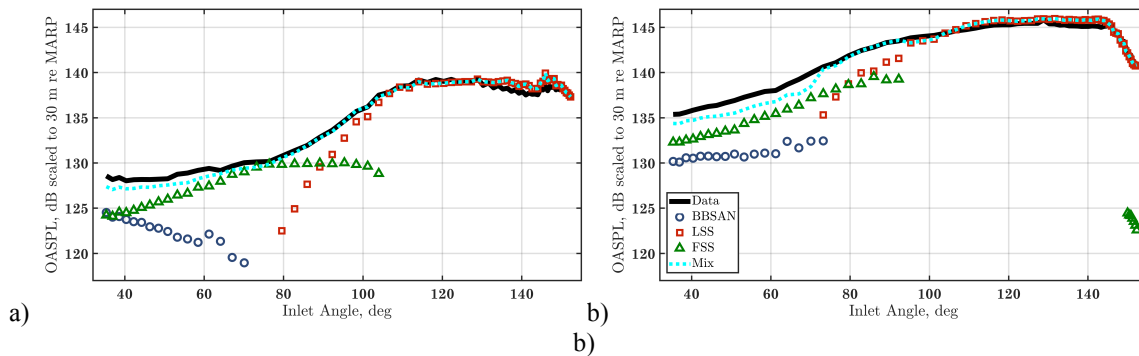


Figure 7. Comparison of the F-35B OASPL (black) at (a) 75% ETR and (b) 150% ETR to the OASPL of the modeled spectral components: LSS (red), FSS (green), BBSAN (blue), and the combination of the three (cyan).

The peak frequencies associated with the three spectral models also change as a function of angle. As shown in Figure 8, the trends differ for each spectral model. The peak frequency of the BBSAN model increases with inlet angle: from 570 Hz at 35° to approximately 1250 Hz at 70° for 75% ETR (Figure 8(a)) and from 390 Hz at 35° to approximately 850 Hz at 70° for 150% ETR (Figure 8(b)). In contrast, the peak frequency of the FSS spectrum remains constant across the entire angular range, both at smaller inlet angles and when it re-emerges aft of the maximum radiation region. For 75% ETR, the LSS spectrum's peak frequency begins at 320 Hz around 80° and remains approximately constant over the combination region (80°-105°). In the maximum radiation region, the peak frequency of the LSS spectrum decreases and then levels off around 100 Hz for $\theta > 140^\circ$. At 150% ETR, a continually decreasing peak frequency is used for the LSS spectrum from 800 Hz at 70° to 50 Hz at 152°. These trends resemble the peak-frequency analysis of a different high-performance military aircraft engine shown in Ref. [33], as well as the variation in peak frequency shown for the high-temperature, laboratory-scale jet noise studies by Seiner *et al.* (See Figure 16 of Ref. [40]). Closest to the jet axis for 150% ETR, after the strength of the large-scale turbulent mixing noise has diminished and its peak frequency has shifted low enough, the PSD is better matched by adding the FSS spectrum at a similar peak frequency used present for the sideline and combination regions.

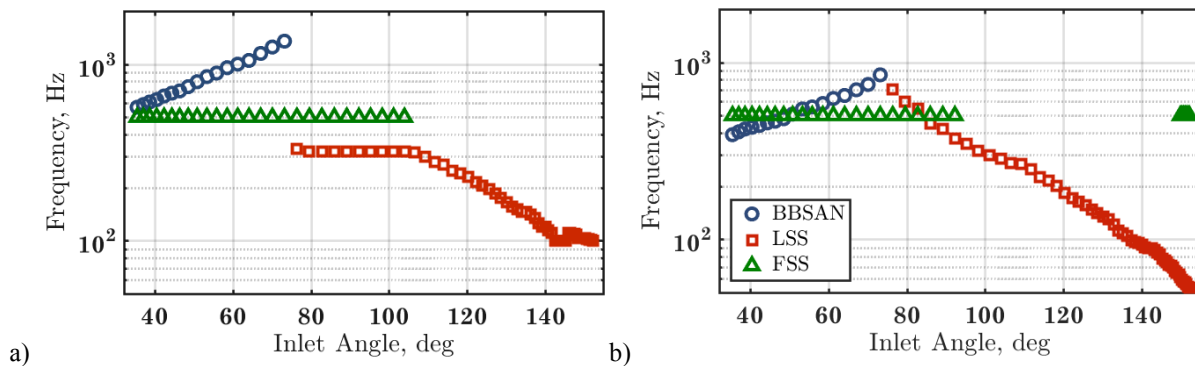


Figure 8. Spatial variation in peak frequency of BBSAN (blue), FSS (green), and LSS (red) spectra.

B. Errors

A concise way to view the overall performance of the three-way decomposition is with spatio-spectral error maps. These maps (Figure 9) contain the difference between the F-35B PSD measured on the ground-based array and those predicted by the combined LSS, FSS, and BBSAN spectral models; these maps highlight spatial and frequency-dependent regions where the spectral decompositions do and do not agree well with the measurements. Again, 75% ETR is on the left (a) and 150% ETR is on the right (b). Many regions have remarkable agreement with ± 2 dB error between the measured and modeled PSD. This agreement indicates that the combination of the turbulent mixing noise similarity spectra and Kuo *et al.*'s BBSAN model account for large portions of the radiated sound. The regions with higher error correspond to limitations of using these spectral models for high-performance military aircraft noise.

The largest positive errors occur at high frequencies in the maximum radiation direction, where the measured spectral levels are higher than LSS spectrum. The sound levels received in this region (roughly 100° to 145°) are sufficiently large for cumulative nonlinear propagation to steepen the pressure waves and, thus, change the high-frequency spectral slope from the -28 dB/decade predicted by the LSS spectrum towards the -20 dB/decade slope associated with nonlinear propagation [39]. This change is greatest at the highest frequencies and affects progressively lower frequencies over a wider angular aperture as ETR increases. Evidence for cumulative nonlinear propagation effects for the tied-down F-35 is presented in Refs. [48,49]. The differing high-frequency slope confirm what was reported for a different aircraft engine's noise in Ref. [33].

In the forward direction (low values of θ), the high-frequency measured spectral levels are also larger than the modeled values. Higher-frequency BBSAN components cause the extra energy seen around 1000 Hz for $\theta < 50^\circ$. A preliminary attempt to model higher-frequency components of the BBSAN is presented in Sec. V.E. At frequencies around 10 kHz and higher, the extra energy in the measured spectra could also be due to waveform steepening. The laboratory-scale jet noise study in Ref. [5] provides evidence of nonlinear propagation effects at $\theta = 35^\circ$ for heat-simulated, supersonic, laboratory-scale jet. Previous analyses of high-performance military aircraft noise indicate the presence of nonlinear propagation for small inlet angles. A high-frequency spectral slope of $1/f^2$ (as expected for shock-containing waveforms) is reported in Fig. 6 of Ref. [33]. At 150% ETR for the F-35B measurements used in this paper, the skewness of the time-derivative of the pressure waveforms at forward locations have values larger than five in Fig. 5 of Ref. [49]—a significant value as analytical work has shown that a threshold of five indicates the presence of acoustic shocks [51].

Two possible explanations arise as to why this shallower high-frequency slope is not observed in the middle angular region (roughly centered around 85°). First, it is possible that the combination of the LSS and FSS spectra used in this angular range provides enough flexibility to fit the spectral changes due to waveform steepening. This possibility is constrained by the fairly strict requirements of smoothly varying OASPL and constant peak frequency for the FSS spectrum that guide the fitting process. Second, the low field coherence in this mixing region likely reduces the rate at which the waveform steepening occurs. The field coherence for a different military aircraft engine was shown in Ref. [18] and is being shown for the F-35B in Ref. [45]. The low coherence explanation for the lack of waveform steepening would also perhaps explain why the smallest inlet angles again have a shallower high frequency slope: the strong BBSAN component of the noise in that region is likely highly correlated.

At the largest inlet angles, the high-frequency portion of the spatio-spectral maps show less error. For the 75% ETR case, there is less error for $\theta > 145^\circ$ relative to the LSS spectrum. This decrease in spectral error agrees with the decreases in nonlinear propagation effects in this region quantified with different nonlinearity metrics by Reichman *et al.* [49]. A similar decrease in error is seen around $140^\circ - 145^\circ$ at 150% ETR. For larger θ , however, there is a distinctive shift in the high-frequency spectral slope—a kink—at which point the FSS spectrum is again added to the spectral model. This downstream combination region occurs aft of a location when the LSS spectrum matches large portions of the high-frequency slope [14,33]. For the higher engine powers, the maximum radiation region for the large-scale turbulent mixing noise has shifted farther from the jet axis (Figure 7b) and has a significantly lower peak frequency (Figure 8b), such that the fine-scale mixing noise can be detected in the spectral shape. The addition of the FSS spectrum aft of the maximum radiation region at high engine powers follows the work in Ref. [14]; the combination of the LSS and FSS spectra—with the same peak frequency for the FSS spectrum as at smaller θ (Figure 8b)—improves the high-frequency fit.

Looking now at the middle frequency range on Figure 9, the negative errors in the 100-800 Hz range (between 110° and 145°) come from dips in the measured PSD between the multiple frequency peaks (Figure 6(a)). In the spatio-spectral error maps in Figure 9, these dips are seen as striations and correspond to multiple spectral peaks occurring at different angles in the maximum radiation region. These multiple spectral peaks are a manifestation of the multiple spatial lobe that have been observed in the sound field around high-performance military aircraft. Evidence for and characterization of these multiple lobes are given in Refs. [14,33,18,52] for a different aircraft engine and in Refs. [44,45] for the F-35B measurements used in this paper.

The large positive errors below 100 Hz in the maximum radiation region are a curious feature. These errors correspond to the fact that the LSS spectral slope below the peak frequency is shallower than is observed in the measurements. Examples of this at 75% ETR are shown in Figure 6. This low-frequency discrepancy was also observed in Refs. [14, 15] for different aircraft engines but not in laboratory-scale jet spectral decompositions in Refs. [53] (performed by the authors using the same methods as in this paper). The reason for the steep low-frequency slope in the maximum radiation region at both 75% and 150% ETR is unknown at the present time, but it appears to persist

into the far field, as shown in Figs. 4 and 5 of Ref. [37]. Similarly, the errors seen in the 150% ETR case at low frequencies for small inlet angles are not yet accounted for.

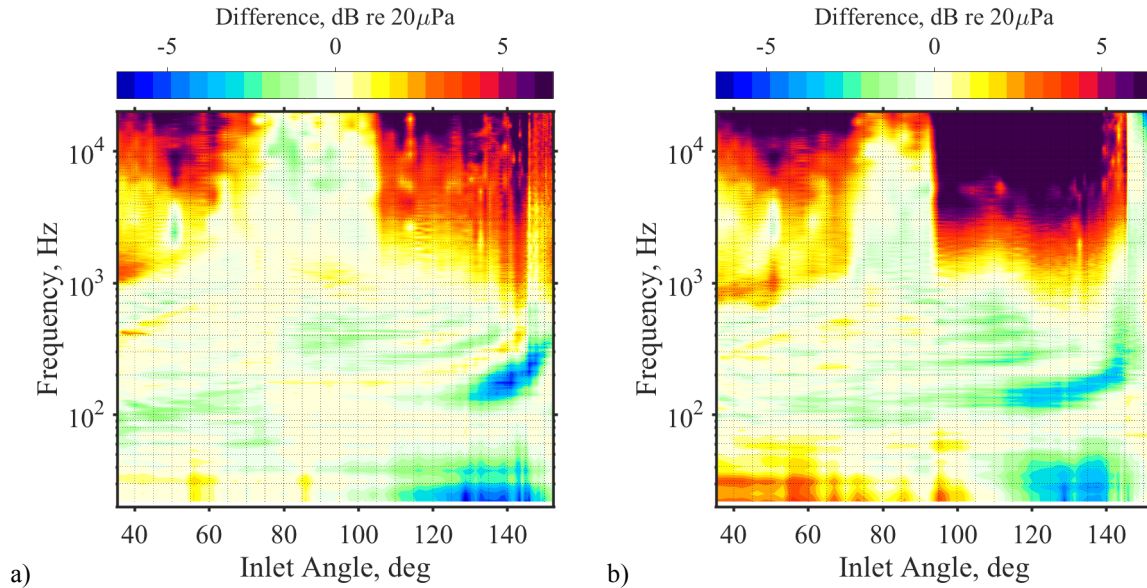


Figure 9. Spatospectral error maps of the three-way decomposition (FSS+LSS+BBSAN) compared to the measured PSD on the 71 ground-based microphones at 75% ETR (left) and 150% ETR (right).

C. Four characteristics of BBSAN

In nonideally expanded, laboratory-scale jet noise, as well as in theoretical models, BBSAN has four distinctive characteristics. Some questions exist as to if these characteristics hold for BBSAN from high-performance military aircraft. Vaughn *et al.* [30] shows the spatial variation in F-35B BBSAN peak level, frequency, and width at 75%, 100%, 130%, and 150% ETR across the ground-based array. In the current analysis, the BBSAN model parameters for the afterburning conditions (130% and 150% ETR) are compared to those reported for a tied-down F/A-18E reported by Tam *et al.* in Ref. [16]. While some of the BBSAN characteristics are the same as the laboratory-scale BBSAN, others are quite different; the F-35B and F/A-18E BBSAN modeling efforts currently lead to different conclusions. A direct comparison is provided between the two sets of results.

The most identifiable BBSAN characteristic is the distinctive spectral shape that is steeper on the low-frequency side of the peak than on the high-frequency side. Possible spectral models for this shape are described in Sec II.B. The distinctive BBSAN spectral shape is seen in both the F-35B BBSAN (see Figure 4(a)) and F/A-18E BBSAN (shown in Fig. 13 of Ref. [16].)

The second BBSAN property of interest is the peak frequency. In nonideally expanded, laboratory-scale jets, the BBSAN peak frequency increases as inlet angle increases. Early researchers related this increase in peak frequency to constructive interference [4] and perhaps a Doppler effect, at least qualitatively [20]. More recently this shift in peak frequency has been explained by Tam's wavy wall analogy [21,29]. In agreement with laboratory-scale observations, the measured F-35B BBSAN at 75%, 100% 130% and 150% ETR all show this same increase in peak frequency with inlet angle. For comparison, the afterburning F-35B BBSAN f_{peak} are displayed in Figure 10(a) along with those reported in Table 2 of Ref. [16] for the afterburning F/A-18E BBSAN; both agree with the laboratory-scale trend.

The third BBSAN characteristic is the peak spectral level, L_{peak} . In laboratory-scale measurements of BBSAN, L_{peak} decreases as inlet angle increases. In Ref. [30], it is shown that L_{peak} follows this same trend for F-35B BBSAN at 75% ETR, but not for higher ETR. For the F-35B engine at afterburner (after scaling to a common distance), L_{peak} first increases slightly then decreases; the change in L_{peak} with inlet angle, relative to the maximum level at each afterburning ETR, is shown in Figure 10(b). The total change in L_{peak} across the angular aperture is less than 4 dB, but as PSD from repeated measurements deviated by only 1 dB, the 4 dB change can be considered a physical features of the afterburning F-35B BBSAN. In contrast, the afterburning F/A-18E L_{peak} (from Table 2 of Ref. [16]) increases by less than 2 dB as inlet angle increases over an angular range of 35° - 65° . No indication is given as the uncertainty

associated with the F/A-18E levels, and it is puzzling that the authors used only four measurement locations to identify a contrary trend of increasing L_{peak} since seven points are used to confirm the trend of increasing peak frequency. It is only the last of the F/A-18E points that does not follow the trends of the F-35B L_{peak} . The conclusion for the afterburning F-35B BBSAN is that L_{peak} increases slightly (from 35° to approximately 50°) and then decreases, with the latter part agreeing with laboratory-scale data.

The fourth BBSAN characteristic is the width of the BBSAN spectral model (w_{sh} in Eq. (4)). In nonideally expanded, laboratory-scale jets, this width increases as inlet angle increases. The afterburning F/A-18E BBSAN was reported to have the opposite behavior: the width decreases as inlet angle increases. The F/A-18E widths (from Table 2 of Ref. [16]) are compared to the afterburning F-35B in Figure 10(c). For the F-35B, w_{sh} increases as the inlet angle increases from 35° to approximately 50° and then decreases at larger inlet angles. There is remarkable agreement between w_{sh} of the F-35B at 150% ETR and the first three F-18E measurement locations, but w_{sh} reported for the fourth location differs greatly; the reason for this difference is unknown. The trend of decreasing then increasing w_{sh} , shown here for the F-35B afterburning cases, is also observed at 75% and 100% ETR [30]. The decrease in width of the F-35B BBSAN over an approximate angular aperture of 35° to 50° occurs at the same angles that L_{peak} increases and is opposite the expected laboratory-scale trend. Additional investigation is required to determine the cause. To summarize the similarities and difference between laboratory and full-scale jets, the trends for each characteristic are compiled in

Table 1. In all cases, the BBSAN is observed in the forward and sideline directions and has the same distinctive spectral shape and increase in peak frequency as the inlet angle increases. However, the trends in peak level and width used in the BBSAN spectral model are reportedly different between the three cases.

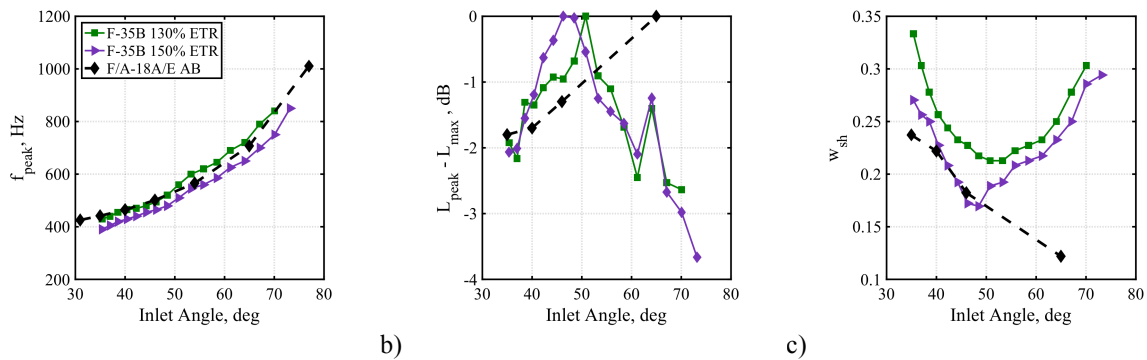


Figure 10. Comparison of (a) f_{peak} , (b) L_{peak} relative to the maximum at each engine condition, and (c) width parameter q used in Eq. (4) for the F-35B at minimum (green squares) and maximum (and purple triangles) afterburner and the values for the F/A-18E at afterburner (black diamonds) reported in Refs. [16].

Table 1. Comparison between trends in BBSAN features for laboratory-scale jets, the afterburning F-35B, as reported in this paper, and the afterburning F/A-18E reported in Ref. [16].

Lab-scale BBSAN	F-35B BBSAN	F/A-18E BBSAN
Sideline & Forward direction	Yes	Yes
Distinctive Shape	Yes	Yes
f_{peak} increases with θ	Yes	Yes
L_{peak} decreases with θ	Increases then decreases	Increases
w_{sh} increases with θ	Decreases then increases	Decreases

D. Estimates of convective velocity

In addition to the above trends in L_{peak} and w_{sh} not matching laboratory-scale BBSAN studies, it appears that the application of Eq. (1) to high-performance military aircraft noise, or at least the interpretation thereof, is not straightforward. In this section, frequency-dependent convective velocity estimates obtained from Eq. (1) are compared to estimates based on far-field directivity. When placed in Eq. (1), the collection of measured f_{peak} as a function of θ (shown in Figure 10(b)) yield a system of equations that can be solved via a least-squares method for u_c and L . For the F-35B at 150% ETR, the resulting estimated values are $u_c = 1620$ m/s and $L = 0.8$ m, similar to $u_c = 1435$ m/s and $L = 0.7$ m for the F/A-18E afterburning case in Ref. [16]. While the values of L seem reasonable, the estimates of u_c are much larger than expected from the far-field directivity. A measurement arc located at 76 m (250 ft) from the MARP for the F-35B case, has peak directivity angles between 125 and 140°, corresponding to convective speeds of 450-600 m/s, significantly lower than those estimated via the least-squares solution based on the BBSAN peak frequencies and Eq. (1).

There are a few possible reasons for this discrepancy. As postulated in Ref. [16], this could be a new noise mechanism, perhaps related to indirect combustion noise. A different interpretation is that the high-performance military engine noise, especially at afterburner, reaches conditions (rarely seen in laboratory-scale measurements) in which three types of Mach waves are present. The corresponding Mach numbers for these three types of Mach waves were given by Oertel [41], and a theoretical basis for them was presented in Tam and Hu [42]. Seiner *et al.* [40] showed that while the Kelvin-Helmholtz instability waves dominate the noise generation at lower jet temperatures, at higher temperatures, a second type of Mach wave, referred to as the supersonic instability wave, appears. The third type of Mach wave was subsonic in all prior laboratory-scale studies. Possibly the different types of Mach waves are being generated by the exhaust of an afterburning military aircraft engine and interacting with the shock cells in a manner that negates the applicability of Eq. (1). Further investigation is needed to determine how the variation in f_{peak} as a function of θ is related to the convective velocities of these different types of Mach waves.

E. Higher-frequency BBSAN

The final analysis is a preliminary investigation into higher-frequency components of BBSAN that can be seen in the F-35B PSD at the smallest inlet angles. In the Harper-Bourne and Fisher model [4], higher harmonics of BBSAN were proposed but not evident in their data. In the original Tam model for the BBSAN spectrum [27,28], the higher-frequency BBSAN corresponds to higher-order modal frequencies of the waveguide created by the quasi-periodic shock cell structure, as described in Sec. II.B. When the second mode from Tam's model was used in the spectral decomposition of the F-35B noise, it did not produce a reasonable match to the PSD. The method for fitting the second BBSAN component that appears to be more successful is to use Kuo *et al.*'s BBSAN model [29] but for a second harmonic that is wider by a factor of $\sqrt{2}$; the parameters $f_{\text{peak},2} = 2f_{\text{peak}}$ and $w_{\text{sh},2} = \sqrt{2}w_{\text{sh}}$ are used in Figure 11 to generate a spectral model for the same angle as displayed in the left plot of Figure 4. The second harmonic significantly increases the agreement between the measured and modeled spectral levels over the 1000-3000 Hz band. It is possible that additional higher components could potentially improve the fit at higher frequencies. This preliminary investigation shows that further work should be done in developing a model for the higher frequency components of BBSAN for high-performance military aircraft noise.

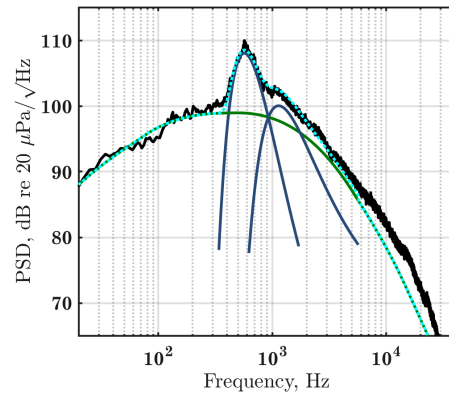


Figure 11 F-35B PSD at 75% ETR (black) decomposed into FSS spectrum (green) and BBSAN first and second harmonics (blue) with the total modeled PSD (cyan) at an inlet angle of 35.4°.

VI. Conclusions

A spectral decomposition has been applied to measurements near a tied-down F-35B that accounts for turbulent mixing noise and broadband shock-associated noise and provides insights into the spatial variation in noise from a high-performance military aircraft engine. Many of the observations from the one-third octave band spectral decomposition of the turbulent mixing noise from measurements near a different full-scale jet aircraft [14] have been confirmed. Over a small angular range the FSS spectrum matches the F-35B spectral density. Slightly farther downstream, a combination of the LSS and FSS spectra matches the F-35B spectral density and the LSS spectrum alone matches just outside the maximum radiation region. In the maximum radiation region, however, the LSS spectrum captures only the overall shape of the F-35B spectral density. The LSS spectrum does not account for the multiple spectral peaks seen in the maximum radiation region. In addition, the high-frequency slope of the F-35B spectral density is shallower than the LSS spectral shape because of nonlinear propagation [48,49], and the low-frequency slope of the F-35B spectral density is steeper than the LSS spectral shape. The cause of the latter is not yet known, although it was also seen in previous aircraft engine noise measurements [14,15,36]. Aft of the maximum radiation region, the LSS spectrum matches the peak and high-frequency portions of the spectrum. For higher ETR and the farthest downstream locations, the main radiation region shifts forward and the peak frequency is sufficient low such that a second combination region is present: A shift in spectral slope at high frequencies is matched by including the FSS spectrum with the same peak frequency as that observed to the sideline. The spatial accuracy of the spectral decomposition from 20 Hz to 20 kHz have been quantified with error maps that indicate quality of fits and highlight remaining discrepancies. The similarity of these conclusions for the F-35B to the prior spectral decomposition [14] is significant because of the differences of the engines. This detailed view of the F-35B turbulent mixing noise is also the first narrowband application of the similarity spectra to high-performance military aircraft noise.

A spectral decomposition has been applied to measurements near a tied-down F-35B that accounts for turbulent mixing noise and broadband shock-associated noise and provides insights into the spatial variation in noise from a high-performance military aircraft engine. Many of the observations from the one-third octave band spectral decomposition of the turbulent mixing noise from measurements near a different full-scale jet aircraft [14] have been confirmed. Over a small angular range the FSS spectrum matches the F-35B spectral density. Slightly farther downstream, a combination of the LSS and FSS spectra matches the F-35B spectral density and the LSS spectrum alone matches just outside the maximum radiation region. In the maximum radiation region, however, the LSS spectrum captures only the overall shape of the F-35B spectral density. The LSS spectrum does not account for the multiple spectral peaks seen in the maximum radiation region. In addition, the high-frequency slope of the F-35B spectral density is shallower than the LSS spectral shape because of nonlinear propagation [48,49], and the low-frequency slope of the F-35B spectral density is steeper than the LSS spectral shape. The cause of the latter is not yet known, although it was also seen in previous aircraft engine noise measurements [14,15,36]. Aft of the maximum radiation region, the LSS spectrum matches the peak and high-frequency portions of the spectrum. For higher ETR

and the farthest downstream locations, the main radiation region shifts forward and the peak frequency is sufficient low such that a second combination region is present: A shift in spectral slope at high frequencies is matched by including the FSS spectrum with the same peak frequency as that observed to the sideline. The spatial accuracy of the spectral decomposition from 20 Hz to 20 kHz have been quantified with error maps that indicate quality of fits and highlight remaining discrepancies. The similarity of these conclusions for the F-35B to the prior spectral decomposition [14] is significant because of the differences of the engines. This detailed view of the F-35B turbulent mixing noise is also the first narrowband application of the similarity spectra to high-performance military aircraft noise.

The other unique part of this study has been the decomposition of the F-35B sound field at small inlet angles into FSS spectrum and a BBSAN spectral model. BBSAN was not analyzed in the prior study [14]; BBSAN was not evident in the one-third octave band spectra, although ringing in the autocorrelation function at low inlet angles indicated its presence [17,18]. In the narrowband F-35B spectral density, the characteristic BBSAN spectral peak exceeds the fine-scale turbulent mixing noise at inlet angles of 35°-70°. Kuo *et al.*'s model for the BBSAN spectrum [29] matches the main BBSAN peak. The peak frequency of the BBSAN increases with increasing inlet angle, as seen in prior laboratory-scale studies and initial investigation of F/A-18E BBSAN [16]. The other two characteristics seen in laboratory-scale BBSAN—decrease in peak level and increase in width with increasing inlet angle—are not the same as seen for high-performance military aircraft. The peak and level of the F/A-18E BBSAN behaves in an opposite manner, whereas the F-35B BBSAN level first increases then decreases as inlet angle increases from 35° to 70°, with the width exhibiting the opposite: in decreasing the increasing. Another contradiction between the established BBSAN models is that the angular dependence on peak frequency yields estimates of convective speed that are much larger than those derived from the “wavy-wall” analogy based on far-field directivity. This discrepancy was also observed for F/A-18E BBSAN [16]. Additional work is needed to clarify the relationship between the peak frequencies and estimates of the convective velocity and shock cell length, as well as to explore spectral models for higher frequency BBSAN components.

Acknowledgments

The authors gratefully acknowledge funding for the measurements, provided through the F-35B Program Office and Air Force Research Laboratory. Distribution A: Approved for public release; distribution is unlimited. F-35 PAO cleared 04/23/2018; JSF18-414). Analysis was supported in part through a grant from the Office of Naval Research Grant N000141410494.

References

- ¹ Tam, C. K. W., "Supersonic Jet Noise," *Annual Review of Fluid Mechanics*, Vol. 27, 1995, pp. 17-43.
- ² Tam, C. K. W., "Jet Noise: Since 1952," *Theoretical and Computational Fluid Dynamics*, Vol. 10, 1998, pp. 393-405.
- ³ Viswanathan, K., "Aeroacoustics of Hot Jets," *Journal of Fluid Mechanics*, Vol. 516, 2004, pp. 39-82.
- ⁴ Harper-Bourne, M., and Fisher, M. J., "The Noise from Shockwaves in Supersonic Jets," AGARD CP-131, 1974, pp.11.1-11.13.
- ⁵ Petitjean, B. P., Viswanathan, K., and McLaughlin, D. K., "Acoustic pressure waveforms measured in high speed jet noise experiencing nonlinear propagation," *International Journal of Aeroacoustics*, Vol. 5, No. 2, 2006, pp. 193-215.5
- ⁶ R. H. Schlinker, *Supersonic jet noise experiments* (Ph. D. Dissertation, University of Southern California, 1975).
- ⁷ J. Laufer, R. Schlinker, and R. E. Kaplan, "Experiments on supersonic jet noise", *AIAA Journal*, Vol. 14, 1976, pp. 489-498.
- ⁸ Tam, C. K. W., Viswanathan, K, Ahuja, K. K., and Panda, J. "The Sources of Jet Noise: Experimental Evidence," *Journal of Fluid Mechanics*, Vol. 615, 2008, pp. 253-292.
- ⁹ K. Viswanathan, "Analysis of the two similarity components of turbulent mixing noise", *AIAA Journal*, Vol. 40, 2002, pp. 1735-1744.
- ¹⁰ Tam, C. K. W., Golebiowsky, M., and Seiner, J. M., "On the Two Components of Turbulent Mixing Noise from Supersonic Jets," AIAA Paper No. 96-1716, May 1996.
- ¹¹ Tam, C. K. W. and Zaman, K., "Subsonic Noise from Nonaxisymmetric and Tabbed Nozzles," *AIAA Journal*, Vol. 38, 2000, pp. 592-599.
- ¹² Viswanathan, K. "Aeroacoustics of Hot Jets," *Journal of Fluid Mechanics*, Vol. 516, 2004, pp. 39-82.
- ¹³ Schlinker, R. H., Liljenberg, S. A., Polak, D. R., Post, K. A., Chipman, C. T., and Stern, A. M., "Supersonic Jet Noise Source Characteristics & Propagation: Engine and Model Scale," AIAA Paper 2007-3623, 2007.
- ¹⁴ Neilsen, T. B., Gee, K.L., A.T. Wall, and M.M. James, "Similarity Spectra Analysis of High-performance Jet Aircraft Noise," *Journal of the Acoustical Society of America*, Vol. 133, No. 4, 2013, pp. 2116-2125. DOI: 10.1121/1.4792360
- ¹⁵ Neilsen, T. B., Gee, K. L., Wall, A. T., James, M. M., and Atchley, A. A., "Comparison of Supersonic Full-scale and Laboratory-scale Jet Data and the Similarity Spectra for Turbulent Mixing Noise," *Proceedings of Meetings on Acoustics*, Vol. 19, 2013, 040071.
- ¹⁶ Tam, C. K. W., Aubert, A. C., Spyropoulos, J. T., Powers, R. W., "On the dominant noise components of tactical aircraft: Laboratory to full scale," *Journal of Sound and Vibration*, Vo. 422, 2018, pp. 92-111. DOI: 10.1016/j.jsv.2018.02.023
- ¹⁷ B. M. Harker, K. L. Gee, T. B. Neilsen, A. T. Wall, S. A. McNerny, and M. M. James, "On autocorrelation analysis of jet noise," *Journal of the Acoustical Society of America*, Vol. 133, 2013, pp. EL458 – EL464.
- ¹⁸ Harker, B. M., Neilsen, T. B., Gee, K. L., Wall, A. T., and James, M. M., "Spatiotemporal Correlation Analysis of Jet Noise from a High-Performance Military Aircraft," *AIAA Journal*, Vol. 54, No. 5, 2016, pp. 1554-1566.
- ¹⁹ Faranosov, G.A., Belyaev, I.V., Kopiev, V.F., Zaytsev, M.Y., Aleksentsev, A.A., Bersenev, Y.V., Chursin, V.A. and Viskova, T.A., "Adaptation of the Azimuthal Decomposition Technique to Jet Noise Measurements in Full-Scale Tests," *AIAA Journal*, Vol. 55, No. 2, 2017, pp. 572-584. DOI: 10.2513/1.J055001
- ²⁰ Seiner, J. M. and Norum, T. D., "Experiments of Shock Associated Noise of Supersonic Jets," AIAA Paper 1979-1526, 1979.
- ²¹ Norum, T. D., and Seiner, J. M., "Broadband Shock Noise from Supersonic Jets," *AIAA Journal*, Vol. 20, 1982, pp. 68-73.
- ²² Seiner, J. M., and Yu, J. C., "Acoustic Near-Field Properties Associated with Broadband Shock Noise," *AIAA Journal*, Vol. 22, No. 9, 1984, pp. 1207-1215.
- ²³ Tanna, H. K., "An experimental study of jet noise part ii: shock associated noise," *Journal of Sound and Vibration*, Vol. 50, No. 3, 1977, pp. 429-444.
- ²⁴ Pao, S. P., and Seiner, J. M., "Shock-Associated Noise in Supersonic Jets," *AIAA Journal*, Vol. 21, No. 5, 1983, pp. 687-693. DOI:10.2514/3.8134

-
- ²⁵ Panda, J., and Seasholtz, R. G., "Measurements of Shock Structure and Shock-Vortex Interaction in Underexpanded Jets Using Rayleigh Scattering," *Physics of Fluids A: Fluid Dynamics*, Vol. 11, No. 12, 1999, pp. 3761–3777. DOI:10.1063/1.870247
- ²⁶ Tam, C. K. W., and Tanna, H. K., "Shock Associated Noise of Supersonic Jets from Convergent-divergent Nozzles," *Journal of Sound and Vibration*, Vol. 81, 1982, pp. 337-358.
- ²⁷ Tam, C. K. W., "Stochastic Model Theory of Broadband Shock Associated Noise from Supersonic Jets," *Journal of Sound and Vibration*, Vol. 116, 1987, pp.265-302.
- ²⁸ Tam, C. K. W., "Broadband Shock Associated Noise of Moderately Imperfectly Expanded Supersonic Jets," *Journal of Sound and Vibration*, Vol. 140, 1990, pp. 55-71.
- ²⁹ Kuo, C. W., McLaughlin, D. K., Morris, P. J., and Viswanathan, K., "Effects of Jet Temperature on Broadband Shock-associated Noise," *AIAA Journal*, Vol. 53, 2015, pp. 1515-1530.
- ³⁰ Vaughn, A. B., Neilsen, T. B., Gee, K. L., Wall, A. T., Downing, J. M., James, M. M., "Broadband shock-associated noise of a high-performance military aircraft," *Journal of the Acoustical Society of America – Express Letters* (in preparation).
- ³¹ Viswanathan, K., Alkisar, M. B., and Czech, M. J., "Characteristics of the Shock Noise Component of Jet Noise," *AIAA Journal*, Vol. 48, 2010, pp. 25-46. DOI: 10.2514/1.38521
- ³² Viswanathan, K., "Scaling Laws and a Method for Identifying Components of Jet Noise," *AIAA Journal*, Vol. 44, 2006, pp. 2274-2285.
- ³³ Neilsen, T. B., Gee, K. L., and James, M. M., "Spectral Characterization in the Near and Mid-field of Military Jet Aircraft Noise," AIAA paper 2013-2191, June 2013.
- ³⁴ Wall, A. T., Gee, K. L., James, M. M., Bradley, K. A., McNerny, S. A., and Neilsen, T. B., "Near-field Noise Measurements of a High-performance Military Jet Aircraft," *Noise Control Engineering Journal*, Vol. 60, 2012, pp. 421-434.
- ³⁵ Petitjean, B. P. and McLaughlin, D. K., "Experiments on the Nonlinear Propagation of Noise from Supersonic Jets," AIAA Paper 2003-3127, 2003
- ³⁶ Gee, K. L., Gabrielson, T. B., Atchley, A. A. and Sparrow, V. W., "Preliminary Analysis of Nonlinearity in Military Jet Aircraft Noise Propagation," *AIAA Journal*, Vol. 43, No. 6, 2005, pp. 1398-1401.
- ³⁷ Gee, K. L., Sparrow, V. W., James, M. M., Downing, J. M., Hobbs, C. M., Gabrielson, T. B., and Atchley, A. A. "The Role of Nonlinear Effects in the Propagation of Noise from High-power Jet Aircraft," *The Journal of the Acoustical Society of America* Vol. 123, No. 6, 2008, pp. 4082-4093.
- ³⁸ Gee, K. L., Neilsen, T. B., Downing, J. M., James, M. M., McKinley, R. L., McKinley, R. C., and Wall, A. T., "Near-field Shock Formation in Noise Propagation from a High-power Jet Aircraft," *Journal of the Acoustical Society of America*, Vol. 133, No. 2, 2013, EL88 – EL93.
- ³⁹ Gee, K. L., Neilsen, T. B., Wall, A. T., Downing, J. M., James, M. M., McKinley, R. L., "Propagation of Crackle-containing Noise from Military Jet Aircraft," *Noise Control Engineering Journal*, Vol. 64, 2016, pp. 1-12. DOI: [10.3397/1/376354](https://doi.org/10.3397/1/376354)
- ⁴⁰ Seiner, J.M., Ponton, M. K., Jansen, B. J., and Lagen, N. T., "The Effects of Temperature on Supersonic Jet Noise Emission," AIAA Paper 92-02-46, May 1992, p. 295-307.
- ⁴¹ Oertel, H., "Measured Velocity Fluctuations Inside the Mixing Layer of a Supersonic Jet," *Recent Contributions to Fluid Mechanics*, edited by W. Haas, Springer, Berlin, Heidelberg, 1982, pp. 170-179. DOI: [10.1007/978-3-642-81932-2_18](https://doi.org/10.1007/978-3-642-81932-2_18)
- ⁴² Tam, C. K. W. and Hu, F. Q., "On the Three Families of Instability Waves of High-speed Jets," *Journal of Fluid Mechanics*, Vol. 201, No. 4, 1989, pp. 447-483. DOI: [10.1017/S002211208900100X](https://doi.org/10.1017/S002211208900100X)
- ⁴³ Wall, A T., Leete, K. M., Gee, K. L., Neilsen, T. B., James, M. M., and McKinley, R. L., "Preliminary Investigation of Multilobe Fighter Jet Noise Sources Using Acoustical Holography," AIAA Paper 2017-3520, June 2017.
- ⁴⁴ Leete, K. M. Wall, A T., Gee, K. L., Neilsen, T. B., James, M. M., and J. M. Downing, "Dependence of High-performance Military Aircraft Noise on Frequency and Engine Power," submitted to AIAA Aviation 2018, June 2018.
- ⁴⁵ Swift, H. S., Gee, K. L., Neilsen, T. B., Wall, A. T., Downing, J. M., and James, M. M., "Spatiotemporal Correlation Analysis of Jet Noise from a Round-nozzle Supersonic Aircraft," submitted to AIAA Aviation 2018, June 2018.

⁴⁶ Liu, J., Corrigan, A., Kailasanath, K., and Taylor, B., "Impact of the Specific Heat Ratio on Noise Generation of a High-temperature Supersonic Jet," AIAA 2016-2125, January 2016.

⁴⁷ James, M. M., Salton, A. R., Downing, J. M., Gee, K. L., Neilsen, T. B., Reichman, B. O., McKinley, R. L., Wall, A. T., and Gallagher, H. L., "Acoustic Emissions from F-35B Aircraft during Ground Run-Up," AIAA paper 2015-2375, June 2015.

⁴⁸ Reichman, B. O., Wall, A. T., Gee, K. L., Neilsen, T. B., Downing, J. M., James, M. M., and McKinley, R., "Modeling Far-field Acoustical Nonlinearity from F-35B Aircraft During Ground Run-up", AIAA Paper 2016-1888, January 2016. DOI: 10.2514/6.2016-1888

⁴⁹ Reichman, B. O., Gee, K. L., Neilsen, T. B., Swift, S. H., Wall, A. T., Gallagher, H. L., Downing, J. M., and James, M. M., "Acoustic Shock Formation in Noise Propagation during Ground Run-up Operations of Military Aircraft," AIAA Paper 2017-4043, June 2017.

⁵⁰ Morris, P. J., "A Note on Noise Generation by Large-scale Turbulent Structures in Subsonic and Supersonic Jets," *International Journal of Aeroacoustics*, Vol. 8, No. 4, 2009, pp. 301–315.

⁵¹ Reichman, B. O., Muhlestein, M. B., Gee, K. L., Neilsen, T. B., Thomas, D. C., "Evolution of the derivative skewness for nonlinearly propagating waves," *Journal of the Acoustical Society of America*, Vol. 139, 2016, pp. 1390-1403. DOI: 10.1121/1.4944036

⁵² Stout, T. A., Gee, K. L., Neilsen, T. B., Wall, A. T., and James, M. M., "Source Characterization of Full-scale Jet Noise Using Acoustic Intensity," *Noise Control Engineering Journal*, Vol. 63, No. 6, 2015, pp.522-536.

⁵³ Vaughn, A. B., Neilsen, T. B., Gee, K. L., Okamoto, K. and Akamine, M., "Near-field Spatial Variation in Similarity Spectra Decomposition of a Mach 1.8 Laboratory-scale Jet," *Proceedings of Meetings on Acoustics*, Vol. 29, 2016, 045004. DOI: 10.1121/2.0000456